Valorization of the poultry litter through wet torrefaction and different activation treatments

P. J. Arauzo[1]*, P. A. Maziarka[2], M. P. Olszewski[1], R. L. Isemin[3], N. S. Muratova[3], F. Ronsse[2], A. Kruse[1]

[1]Department of Conversion Technologies of Biobased Resources, Institute of Agricultural Engineering, University of Hohenheim, Garbenstrasse 9, DE-70599 Stuttgart, Germany

[2]Department of Green Chemistry and Technology, Faculty of Bioscience Engineering, Ghent University, Coupure Links 653, 9000 Gent, Belgium

[3]Biocenter, Biocenter, Tambov State Technical University, Sovetskaya street, 106, Tambov, 392000, Russia.

1. Introduction

The growth in demand of commodities, which results from a growing global population, leads to the depletion of available resources needed for their production. Additional to fossil resources, also those provided by nature like food, land and biomaterials are affected. The increase in the volume of generated waste is directly linked to the growth in commodity production and the associated need for resources. Additionally, from the increase in social-environmental awareness arises a need for the development of novel conversion techniques that can close the material loop and enable the valorization of waste. One of the options is to replace primary materials with valorized wastes (i.e. secondary materials), and simultaneously reduce resource depletion. For example, the production of activated carbons and/or fertilizers from waste fit very well in that scenario.

Activated carbon (AC) has a wide range of applications, especially in industrial uses due to their high surface area and well-developed porosity. These properties make them suitable as catalysis support and for the production of super-capacitors (Rashidi and Yusup, 2017). Moreover, they are suitable as absorbents of pollutants such as chromium and cadmium from aqueous streams (Asadullah et al., 2014) as well as CO_2 from flue gases (Dwivedi et al., 2004). ACs are also used in wastewater treatment plants for the removal of organic micro-pollutants or even nano-pollutants (i.e. pharmaceuticals and complex chemicals), which cannot be handled by conventional systems (Benstoem et al., 2018; Freihardt et al., 2017). The increase in the number of reports on the positive effect of applying carbonaceous materials in agriculture with respect to crop production and soil health gains increasing interest (Li et al., 2020). This opens up possibilities for use of ACs or biochar produced from bio-resources in agriculture, as a sustainable fertilizer and soil enhancer.

The production of ACs consists of two steps. The first is the carbonization of the initial material (precursor) at elevated temperature and in an inert atmosphere (usually nitrogen). Its purpose is to

increase the material's carbon content and reduce its reactivity toward gasification. The second step is the activation, which is a controlled, partial-gasification and/or further carbonization performed to increase the internal surface area of the precursor. The activation can be divided into 3 treatment types depending on the applied conditions: thermal activation (high temperature only), physical activation (high temperature with the supply of oxidising gases) and chemical activation (high temperature and the addition of reactive chemicals). The reason of applying high temperatures during activation treatment is to achieve the completely conversion of the different biopolymers that constitute the biomass. A study carried by Rodriguez et al. (Rodriguez Correa et al., 2019) states that at temperatures up to 600 °C only hemicellulose and cellulose have been completely converted into carbonaceous structure. While the complete decomposition of lignin requires at least a temperature of 800 °C. In case of thermal and physical activation, the carbonaceous material is heated up to temperatures ranging between 600 °C to 1000 °C (Nazem et al., 2020; Osman et al., 2019; Rodriguez Correa et al., 2019). The main difference between thermal activation and physical activation is the composition of the process gas atmosphere. In thermal activation, an inert gas atmosphere is applied, while for the physical activation an oxidising gas (gasifying agent) is added, such as CO_2 or steam. Finally, in chemical activation, the carbonaceous precursor is mixed with a chemical reagent and heated in an inert atmosphere to temperatures ranging between 500 °C and 900 °C (Otowa et al., 1997; Plaza et al., 2012). Various reagents, such as $ZnCl_2$, H_3PO_4, K_2CO_3, Na_2CO_3, $AlCl_3$, KOH or NaOH can be used, leading to different chemical reactions with the precursor (Oginni et al., 2019; Rodríguez Correa et al., 2018; Suhas et al., 2007; Wei et al., 2015). The use of KOH as reagent results on the increment of the surface area and porous volume of AC, which has several applications such as, adsorption of CO_2 (Dissanayake et al., 2020; Wang et al., 2020) and Cd and Pb immobilization in soil (Wang et al., 2020). A study carried by

Otowa et al. (Otowa et al., 1997) states that the optimum char-to-KOH mass ratio is 1: 4, which also corroborated by other studies (Plaza et al., 2012; Zhu et al., 2014).

Fossil materials like hard coal are considered as the conventional feedstock for the production of ACs. Since their application as raw material is not favorable in terms of sustainability, the focus switches to the application of bio-based raw materials. In studies on this topic, most of the research has been done on “clean” biomass feedstock (i.e. having a low ash content) like wood, bamboo and coconut shell (Rodríguez Correa et al., 2018). However, bio-waste feedstock, like animal manure, gains more interest due to its low-cost and large abundance.

The trend of shifting from “clean” biomass to bio-waste feedstock is even more reasonable in the production of activated carbons for agricultural applications. Concerning this novel feedstock for ACs production, special attention is paid to wastes rich in nutrients (compounds containing N, P, K, Ca, Mg) like poultry litter (PL) or swine manure. A special role in the valorization of manure for agriculture applications is related to phosphates, which in 2017 have been put on the list of critical raw materials in the EU. Manures in the unprocessed form have fertilising properties, but their use bears food safety and environmental concerns (e.g. possible pathogen contamination of vegetable crops) (Chan et al., 2007). It has also been observed that the direct application of unprocessed manure increases the risk of phosphate and nitrate contamination of surface waters (Chan et al., 2008; E. D. Vories et al., 2001). A study carried out by Powell et al., (Powell et al., 2008) shows that thermal treatment reduces the amount of soluble phosphates of the starting material. The thermal treatment of manures also removes its odour and reduces emissions of greenhouse gases in comparison to their direct use (Santos Dalólio et al., 2017). Additionally, biochar produced from manure contains a highly significant amount of nitrogen- and oxygen-containing functional groups on its internal surface, which have a beneficial effect on nutrient

retention in the soil hence increasing their plant availability over longer time periods (Wang et al., 2015).

The valorization of PL, which consists of mainly manure, straw, feathers, and feed residues (Santos Dalólio et al., 2017) *via* chemical or physical activation has not yet been studied in detail. Furthermore, previous studies report that biochar originated from PL, so through thermal activation, has a positive influence on soil quality and crop growth (Cantrell et al., 2012; Chan et al., 2008; Cimò et al., 2014; Enders et al., 2012; J. W. Gaskin et al., 2008; Jeffrey M. Novak et al; Mukome et al., 2013; Pituello et al., 2015). Moreover, the pathogen activity of PL requires a pretreatment for minimizing the bio-hazard risk before the activation treatment. Torrefaction is showed as a possible technology for accomplish it (Isemin et al., 2019). In addition, the high water content of PL (46 wt. %) (Pizarro et al., 2019) makes more suitable the wet torrefaction instead of dry torrefaction because of the elimination of the initial water from the PL would entail a high energy consumption.

This study focuses on the valorization of PL pre-treated with wet torrefaction in a fluidized bed reactor (sanitization purpose). Then, it is activated through different treatments (thermal, physical and chemical) at two different temperatures (600 and 800 °C). The comparison of the physicochemical properties of produced ACs were examined in terms of their use as an absorbent in wastewater treatment systems and soil amendment in agriculture.

2. Method

2.1.Feedstock

The wet torrefied poultry litter (WTPL) used in this this study was provided by Tambov State Technical University Biocenter (Tambov, Russian Federation). It was produced through a wet torrefaction process in a fluidized bed reactor using PL as initial feedstock and described by Isemin

et al. (Isemin et al., 2019). In brief, the installation consists in fluidized bed reactor heated up to 300 °C in a mixture of N_2 gas and steam. Prior to the steam superheater, the flow of steam in saturated state at temperature 117 °C and 0.07 MPa overpressure (Isemin et al., 2019).

2.2. Experimental procedure

2.2.1. Thermal and physical activation

Thermal and physical activation were carried in a fixed bed reactor (a vertical self-made stainless steel reactor 67.0 cm length x 3.8 cm diameter) and experimental setup previously described (Rodríguez Correa et al., 2018). An identical operating procedure of the activation of the precursor and reactor cooling was applied for both mentioned activations. The process started with adding 30g of the WTPL into the reactor. Then, the precursor was activated through heating up to the desired temperature (600 °C or 800 °C) with a heating rate of 10 °C/min under 2 L(STP)/min flow of N_2. Thermal activation was performed by keeping the carbonized precursor at the final temperature for 30 min under a N_2 atmosphere at an unchanged flow rate. For the physical activation, when the desired temperature was reached, the gas was changed from N_2 to CO_2 with a flow rate of 1 L(STP)/min. The carbonised precursor was retained in the reactor at the final temperature and with the flow of oxidising gas for 30 min. During cooling down from final to ambient temperature, the gas was switched to nitrogen at a flow rate of 2 L(STP)/min. The ACs obtained from thermal and physical activation were denoted as Pyro-TTT and CO2-TTT respectively, where TTT is the temperature of activation in Celsius degrees.

2.2.2. Chemical activation

Chemical activation of the WTPL was carried out in nickel crucibles with a volume of 270 ml (BOCHEM, VWR) and experimental setup previously described by (Rodríguez Correa et al., 2018). KOH was used as the activation agent with a char-to-KOH mass ratio of 1:4. The crucibles

were placed in a sealed stainless steel box with a constant flow of N_2 20 L(STP)/min to flush out O_2 and to obtain an inert atmosphere. Then, the box was placed into the muffle furnace, which was pre-heated to the desired final temperature (600 °C or 800 °C) (Nazem et al., 2020; Osman et al., 2019), and the flow of N_2 was reduced to 5 L(STP)/min. After achieving the desired temperature, the box was kept in the oven for 30 min. Afterwards, the box was taken out from muffle furnace to cool down from the operating to ambient temperature and the flow of N_2 was increased to 20 L(STP)/min.

To neutralize unreacted KOH and alkaline compounds resulting from the activation, the previously cooled down AC was mixed with 250 ml of an aqueous solution of 1M HCl (Sigma-Aldrich). Next, the suspension of AC and acid was separated by a quantitative paper filter (grade 413, VWR) placed onto a Büchner flask bottle and connected to a vacuum pump. Prior to the filtration, 5 g of $FeSO_4 \cdot 7\ H_2O$ was put in the Büchner flask to bind hydrocyanic acid that can evolve during the procedure. After the separation of the suspension, the AC was washed on the same setup with warm deionized water to remove the remaining leftovers until the conductivity of the filtrate was lower than 10 µS/cm. The obtained, wet AC was oven-dried overnight at 105 °C. The ACs obtained from chemical activation were labelled as KOH- TTT, where TTT is the temperature of activation in Celsius degrees.

2.3.Characterization of solids

Moisture content, volatile matter (VM), and ash content of the WTPL and ACs were determined according to the standard procedures DIN EN 51718, DIN EN 51720:1978-06, DIN 51719, respectively. Fixed carbon (FC) was calculated by equation (1).

$$FC\ (wt.\%) = 100\% - MC\ (wt.\%) - VM\ (wt.\%) - Ash\ (wt.\%). \quad (1)$$

The elemental composition (C, H, N, S) of the biomass, biochar, and activated carbon was determined by the EURO EA 3000 analyzer (EuroEA 3000 Serie) equipped with a thermal conductivity detector (TCD). According to equation (2), the oxygen content was calculated as follows:

$$O\ (wt.\%) = 100\ \% - N\ (wt.\%) - C(wt.\%) - H(wt.\%) - S(wt.\%) - Ash\ (wt.\%). \quad (2)$$

In advance of the characterization of the surface functional groups of WTPL and activated carbons, they were mixed with potassium bromide (KBr) (1:10 ratio) and pelletized with a force of 20 metric tons. Pellets prepared in such procedure were then analysed in a FTIR spectrophotometer (Bruker ALPHA II PLATINUM-ATR) with wavenumbers ($\tilde{\nu}$) ranging from 4000 cm^{-1} to 400 cm^{-1}.

Inductively coupled plasma optical emission spectrometry (ICP-OES, Agilent Technologies 700 Series) was used to determine the composition of mineral matter in the initial WTPL and ACs. The procedure of measurement was done according to Ovsyannikova et al. (Ovsyannikova et al., 2019).

To measure the pH of the aqueous solution induced by the ACs, 1 g of the investigated sample was mixed with 20 g of deionized water and shaken for 2 h to obtain a stable ionic equilibrium between solid and liquid phase. Then, the obtained suspension was separated by decantation. The pH of the clear filtrate was measured by a HACH HQ40d multi equipment, equipped with the PHC101 pH probe (epoxy, non-refillable gel reference element).

The scanning electron microscope (SEM, Inspect F50; FEI) was used to analyse the morphological structure of the investigated samples. The electron source operated at an excitation voltage of 10 kV. To avoid charging the particles, they were covered with palladium prior to the measurement.

The adsorption of N_2 was measured at its boiling point (-196 °C) and adsorption of CO_2 was measured at 0 °C (Nova 4000e analyzer, Quantachrome Instruments). The activated carbons were degassed at 180 °C for 24h before the adsorption. Data of specific surface area (SSA) was calculated from N_2 adsorption isotherms with the QSDFT method (slit/cylindrical/spherical kernel) and from CO_2 adsorption-desorption isotherms with the GC-MC method. According to the literature, both methods used for calculation in this study are assumed to have the best accuracy and reliability among other methods (Landers et al., 2013; Lowell, 2004; Ravikovitch et al., 2000; Silvestre-Albero et al., 2012). The microporous (pores < 2 nm) and mesoporous (pores from 2 nm to 50 nm) surface area were obtained from the division of the merged dataset from both adsorption measurements on the appropriate pore size ranges.

For the measurement of the absorption capacity of ACs, methylene blue (MB) was used as a reference compound following the procedure of Rodriguez et al. (Rodriguez Correa et al., 2017). In the beginning, 0.1 g of each activated carbon was mixed with 100 ml of MB to result in a concentration of 750 mg/L for 24 h in a shaker (Orbital shaker GFL 301). Applied excessive time for absorption was selected to have certainty that the absorbed quantity of MB reached its maximum (Vargas et al., 2011). Next, the suspension was filtered and the obtained filtrate was used to quantify the MB that had been absorbed on the investigated material. The drop in the concentration of MB was measured using a spectrophotometer (Hach Lange DR6000 UV-Visible spectrophotometer) at the adsorption wavelength of 664 nm. The total quantity of absorbed MB in the sample was calculated according to equation (3):

$$q_e = \frac{(C_0 - C_1) \cdot V}{W}. \quad (3)$$

where

q_e = adsorption of methylene blue in mg /g

C_0 = initial concentration in mg/L

C_1 = equilibrium concentration in mg/L

V = volume of the solution in L

W= amount of activated carbon used for the analysis in g

3. Results

3.1. Chemical properties

The PL was initially pre-processed at a comparatively low temperature (300 °C), at which bio-constituents of the raw material (lignocellulosic bedding, manure, and feathers) can degrade only partially (Katsaros et al., 2020; Atimtay and Yurdakul, 2020). Therefore, the thermal treatment of WTPL at a temperature 600 °C or 800 °C led to further degradation of bio-constituents and material volatilization, and as a consequence, significant mass reduction occurred in every activation experiment. The summary of the yields, proximate and ultimate analysis, and pH of the investigated material is presented in Table 1.

According to previous studies, higher yields of AC should be obtained from the physical and thermal activation in comparison to chemical activation (Prahas et al., 2008; Rodríguez Correa et al., 2018; Saleem et al., 2019). As shown in Table 1, yields of ACs from thermal and physical activation have a value of around 50 wt. %, which is much higher compared to the yields of the chemical activation (6.5 – 15 wt. %). On the other hand, chemical activation results in a strong reduction of the initial WTPL ash content by c.a. 70 % in the resulting ACs. Whilst, the thermal and physical activation treatment doubles the ash content of the WTPL, so there is an extremely inverse influence (Table 1). The application of the strong base, KOH, as the activation agent had

an impact on the composition of the organic matter (Table 1) as well as the inorganic matter of the material (Table 2). At elevated temperatures, the hydroxyl ions of the activation agent are able to react with heteroatoms in the carbonaceous structure. This leads to the release of heteroatoms from the structure in the form of volatiles or easy soluble compounds and consequently increases the carbon content in the processed material (Mau et al., 2018). Silica-alumina can be one of the major compounds that are part of the mineral matter of PL (Shankar Pandey et al., 2019). Silicic acid units, which are the main components of the silica-alumina complex, react with molten hydroxides (KOH) at elevated temperatures. This results in compounds with much higher solubility, like potassium poly-silicates (potassium waterglass). Moreover, neutralisation of the chemically activated carbon with strong acids like HCl enhances the degradation of carbonates and can lead to the formation of highly soluble chloride salts. All above results in an extensive removal of ashes from the chemically activated carbons during washing with warm (60 °C) water.

The yield and parameters of the ACs from the physical and thermal activation show high similarity for the activation at 600 °C, but differences start to appear at 800 °C. This can be related with an increasing influence of the Boudouard reaction and other gasification reactions as it was observed on previous studies (Tang et al., 2020; Wan et al., 2019; Yu et al., 2019). As it was thermodynamically assed by Kwon et al. (Kwon et al., 2013), the free Gibb's energy for the Boudouard reaction is around zero at 710 °C. Therefore, it can be assumed that bellow mentioned temperature the influence of the CO_2 on the solid matter is negligible. Above that temperature the influence of the reaction between carbonaceous material and CO_2 increase its significance. It was also stated by Kwon et al. (Kwon et al., 2015), that the Boudouard reaction does not occur with very rapidly, and it needs time, especially at the temperatures not very far from the temperature at which $\Delta G = 0$. Taking into account that the retention time at 800 °C was relatively short (30 min),

the influence of the solid gasification with CO_2 did not occurred to large extend. Nevertheless, its outcome is distinguishable on yield.

In Table 2, the results of the inorganic composition analysis of investigated materials and initial WTPL are shown. The high concentration of the macro-nutrient forming elements such as N, P, S, K, Ca and Mg allows for the consideration of the material as fertilizer (Font-Palma, 2012). Nevertheless, due to the pre-processing at only 300 °C, the solubility of the phosphorous and nitrogen compounds can be unsatisfactorily high. As a result, the risk of contaminating surface waters during its application as a fertilizer cannot be excluded. In contrast, the phosphorous and nitrogen compounds from ACs, which were produced at much higher temperatures, should have a reduced solubility. The increment of the temperature during the activation of WTPL decreases the content of elements Cu, Mn, and Zn, as they were carried out with the exhaust gases due to the devolatilization of the WTPL (Yang et al., 2015). Moreover, due to a sufficient amount in micro-nutrients (Fe, Mn, Zn, B and Cu), the ACs from thermal and physical activation can be considered as an additive to conventional fertilizers. As indicated on the Table 2, ACs obtained in the physical activation treatment show a slightly lower concentration in environmentally toxic heavy metals (Cr, Pb, Cd) than the ones obtained through thermal activation. It makes the ACs from physical activation more promising in terms of their application in agriculture. Due to treatments during the activation process, the chemically activated ACs have lost most of their valuable nutrients together with their ability to serve as a fertilizer. In addition, those ACs have proven their usability in the adsorption of micro-pollutants in wastewater treatment (Benstoem et al., 2018). To that end, the most promising among the investigated materials are ACs derived from chemical activation due to their low N and P and heavy metal content as well as their high carbon content. Presumably, applying those ACs, in an aqueous environment, will not release a significant load of nutrients/metals over time, and in consequence less contamination of the water will be achieved.

Table 1. Physicochemical properties and pH of WTPL and ACs, yield to ACs. Values are expressed as mean (n = 4), with the standard deviation in brackets.

	Proximate Analysis db [wt. %]			Ultimate Analysis db [wt. %]					Yield of	
	Ash	VM	FC	C	H	N	S	O	char [%]	pH
WTPL	16.87 (0.14)	59.49 (0.50)	23.65 (0.20)	49.10 (0.02)	4.60 (0.01)	5.63 (0.01)	1.44 (0.00)	22.66 (0.01)		6.90 (0.02)
KOH-600	6.20 (0.22)	35.85 (1.26)	57.94 (2.03)	68.42 (1.99)	1.28 (0.14)	1.69 (0.29)	1.11 (0.00)	21.74 (1.50)	14.90 (0.14)	4.86 (0.10)
KOH-800	4.81 (0.05)	19.88 (0.19)	75.31 (0 .73)	83.53 (1.22)	0.22 (0.08)	0.38 (0.10)	1.01 (0.00)	10.15 (1.03)	6.50 (0.68)	6.52 (0.05)
Pyro-600	31.28 (0.43)	24.51 (0.32)	42.16 (0.55)	54.64 (1.22)	0.97 (0.01)	4.74 (0.14)	1.26 (0.24)	7.94 (0.89)	50.83 (0.73)	11.37 (0.06)
Pyro-800	37.09 (0.46)	18.90 (0.25)	46.07 (0.61)	51.86 (1.02)	0.61 (0.02)	4.02 (0.24)	1.09 (0.00)	6.31 (0.78)	48.38 (0.16)	12.66 (0.02)
CO2-600	32.76 (0.49)	25.52 (0.38)	41.72 (0.62)	52.56 (0.98)	1.09 (0.15)	4.14 (0.03)	0.99 (0.01)	9.44 (0.46)	51.17 (0.49)	11.38 (0.05)
CO2-800	35.99 (0.56)	20.17 (0.32)	43.83 (0.69)	51.15 (0.49)	0.82 (0.10)	3.48 (0.11)	1.04 (0.04)	8.65 (1.12)	46.07 (0.61)	12.73 (0.08)

Table 2. Inorganic compounds in initial WTPL and ACs

	S [mg/g]	Al [mg/g]	B [mg/g]	Cd [mg/g]	Ca [mg/g]	Cr [mg/g]	Cu [mg/g]	Fe [mg/g]
WTPL	8.6	0.4	0.0	u.d.	28.9	<0.15	0.4	2.5
KOH-600	2.58	0.70	<0.07	u.d.	16.38	0.03	<0.16	1.68
KOH-800	3.27	0.49	<0.06	u.d.	3.35	0.03	<0.14	0.55
Pyro-600	10.29	0.75	0.09	u.d.	47.64	1.61	0.81	9.76
Pyro-800	11.97	0.87	0.10	u.d.	52.94	0.40	0.87	4.47
CO2-600	9.66	0.81	0.09	u.d.	52.65	0.07	0.83	2.49
CO2-800	10.12	0.83	0.10	u.d.	55.64	0.08	0.94	3.00
	K [mg/g]	Mg [mg/g]	Mn [mg/g]	Na [mg/g]	Ni [mg/g]	P [mg/g]	Pb [mg/g]	Zn [mg/g]
WTPL	30.7	9.7	0.8	3.3	n.d.	20.3	u.d.	0.7
KOH-600	n.d.	4.10	0.63	n.d.	0.04	3.17	u.d.	0.37
KOH-800	n.d.	1.23	0.13	0.66	0.10	0.34	u.d.	0.12
Pyro-600	51.30	16.87	1.50	5.68	1.27	35.41	u.d.	1.20
Pyro-800	57.65	19.21	1.62	6.02	0.33	39.73	u.d.	1.15
CO2-600	55.76	17.48	1.44	6.21	0.07	38.27	u.d.	1.29
CO2-800	60.69	20.25	1.68	6.68	0.11	41.89	u.d.	1.06

*n.d: not detectable, u.d.: under detection limit Cd (0.02 mg/g), Pb (0.24 mg/g)

The FTIR analytical technique was used to characterize functional groups on the surface of produced activated carbons as shown in Figure 1. Stretching vibrations of hydroxyl or carboxyl groups are displayed at $\tilde{\nu}$ = 3500 – 3200 cm^{-1} (Cao and Harris, 2010). The drop in their intensity is visible between ACs and WTPL (Supplementary Figure 1). The minor peak observed only at 2450 – 2350 cm^{-1} in the spectrogram of the ACs physically activated at 800 °C, implies that CO_2 becomes absorbed/trapped inside the carbon structure and exists in it, in a stable form. The wavebands observed at 1700 - 1610 cm^{-1} usually are related to the C=O stretching of carboxyl groups. The increment of the temperature in the activating process, leads to the disappearance of peaks in this range. Such an outcome can be connected to the devolatilization of organic matter, possibly through decarboxylation or elimination of the acidic groups in the form of short carbon-chain acids (Keiluweit et al., 2010). The adsorption peaks between 1560 - 1452 cm^{-1} are assigned to C=C of aromatic structures, whose intensities increase with the rise in activation temperature. Its cause is suspected to be related to polymerization reactions. The ACs produced by physical and chemical treatments shows a peak in the wavelength 1100 – 1000 cm^{-1}, which is assigned to P-O bonds of phosphate, Si-O bonds contained in ash (i.e. SiO_2) (Hossain et al., 2011) and C-O stretching vibration structures. It can be seen that the increment in temperature during the chemical activation produced the disappearance of peaks at this waveband, which is in accordance with P content shown in Table 1. According to Yang et al. (Yang et al., 2015) the peaks appearing below 600 cm^{-1} indicate the presence of metal-halogen (M-X) stretching vibration e.g. chlorate salts. Peaks in this wavenumber are strongly visible for high-ash ACs.

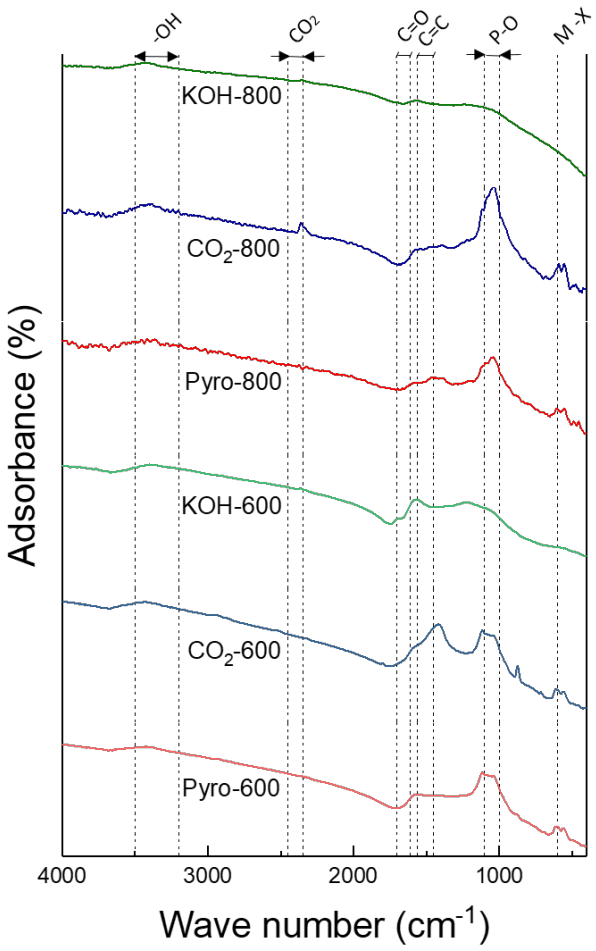

Figure 1. FT-IR of ACs produced with physical and chemical treatments.

The relationship between the pH of the aqueous solution obtained after mixing the ACs with deionized water is not straightforward. A few major parameters have impact on the final outcome of the pH value: the amount of the surface functional groups and their character (acidic or basic), ash content and its composition (Ahmad et al., 2012; Enders et al., 2012; Ippolito et al., 2015; Vassilev et al., 2010; Weber and Quicker, 2018). Changes in the influence of functional groups are related to the activation temperature. With an increase in activation temperature, the amount of the acidic functional groups (carboxyl, hydroxyl, or formyl) decreases due to breaking of the bonds between the heteroatoms (e.g. oxygen, nitrogen) and the carbon rich structure, which leads in

consequence to an increase in aromaticity (Bourke et al., 2007; McBeath et al., 2014; Nishimiya et al., 1998; Ronsse et al., 2015). Generally, pH values in water of untreated biomass are in the range from 5 (weakly acidic) to 7.5 (basically neutral). As a consequence of thermal treatment, the pH value of the solution becomes higher (Vassilev et al., 2010; Weber and Quicker, 2018). Furthermore, a significant amount of ash in the thermally and physically activated carbons has an influence on the pH value of the solution, which cannot be omitted. For those samples, the value of the pH is positively correlated with the ash content. It can lead to the presumption that the high ash concentration can be treated as an indicator of high pH.

Within the most influential components of the ash on the pH value are alkali and alkaline earth metal salts (AAEMs) in which Na, K, Mg and Ca salts play the major roles. A detailed analysis of a wide variety of biochars originated from different biomass (including poultry manure) was made by Enders et al. (Enders et al., 2012). Their study indicates that the concentration of AAEMs is positively correlated with the pH value of the aqueous solution with suspended carbonaceous material ($R^2 = 0.613$, $n = 53$). The study also states that the influence of the temperature (inducing changes in the organic structure) plays a major role in altering the pH only for biomass with a very low ash content (like woody biomass), otherwise the ash content and its composition have the major influence on the pH.

In Table 1, the results of the pH measurement of WTPL and the products of its activations are presented. As already mentioned, the initial PL was pre-treated in a low-temperature process (< 300 °C), i.e. wet torrefaction, and its bio-constituents were not fully converted. This relates especially to cellulose and lignin, whose temperature of thermal degradation is higher than the applied temperature of the wet torrefaction (Giudicianni et al., 2013; Yang et al., 2007). The WTPL has a neutral character (with aqueous pH close to 7). While the remaining functional groups shift

the pH to more acidic, the WTPL's ash content is relatively high and alkaline, thus its influence possibly compensates the acidity. The chemically-treated AC, which was produced at 600 °C, displays acidic behaviour (pH around 5), while with an increase in the temperature to 800 °C, the material's acidity rises to nearly neutral, with the pH value close to 6.5. Presumably, due to the low ash content of ACs activated with KOH (c.a. 5% wt.), the temperature has the strongest influence on pH. Differences in pH between the thermally and physically treated ACs are minor and not visible at the same activation temperature. Thermally and physically activated ACs produced at 600 °C and 800 °C show very high basicity, with a pH around 11.5 and 13, respectively. The major influence on their alkaline pH is assumed to be connected to the high ash, and AAEMs content, whose relative amount increases with production temperature due to the overall decrease in organic matter content (Table 1).

In order to assess if the obtained materials show similar properties to other carbonaceous materials, they were compared with results obtained by Enders et al. (Enders et al., 2012). Figure 2 shows the trend between pH increase in an aqueous solution on one hand and the increase in conversion temperature as well an increasing ash content (wt. %) on the other hand. The comparison of the influence of the conversion temperature (Figure 2, left), shows that ACs obtained from physical and thermal activation present similar behavior with materials whose AAEM content do exceed 5 wt. %. On the other hand, results for the KOH activated ACs show more similarity to materials whose AAEM content was very low (< 2 wt. %). The thermally and physically activated WTPL obtained at 600 °C are comparable in pH of the aqueous solution to that of PL pyrolyzed at 500 °C and 600 °C from Enders et al. (Enders et al., 2012). However, their AAEM concentration is much lower (Figure 2, right). A further increase of the activation temperature by 200 °C of mentioned ACs results in a significant increase in the pH value (by 2 points), without a significant increase of their AAEM's concentration (c.a. 1.2 wt. %). This comparison strongly indicates that for

carbonaceous materials, whose AAEM content is higher than 2 wt.%, not only the concentration but also the ratio of each metal and the form (e.g., carbonate, oxide) in which the AAEM's occurs in the ash, influence the pH of its aqueous solution. For low AAEM containing carbonaceous materials (< 2 wt. %), even a slight increase or reduction of their concentration influences the pH of their solution, due to their much stronger effect than the organic surface groups on the carbonaceous structure.

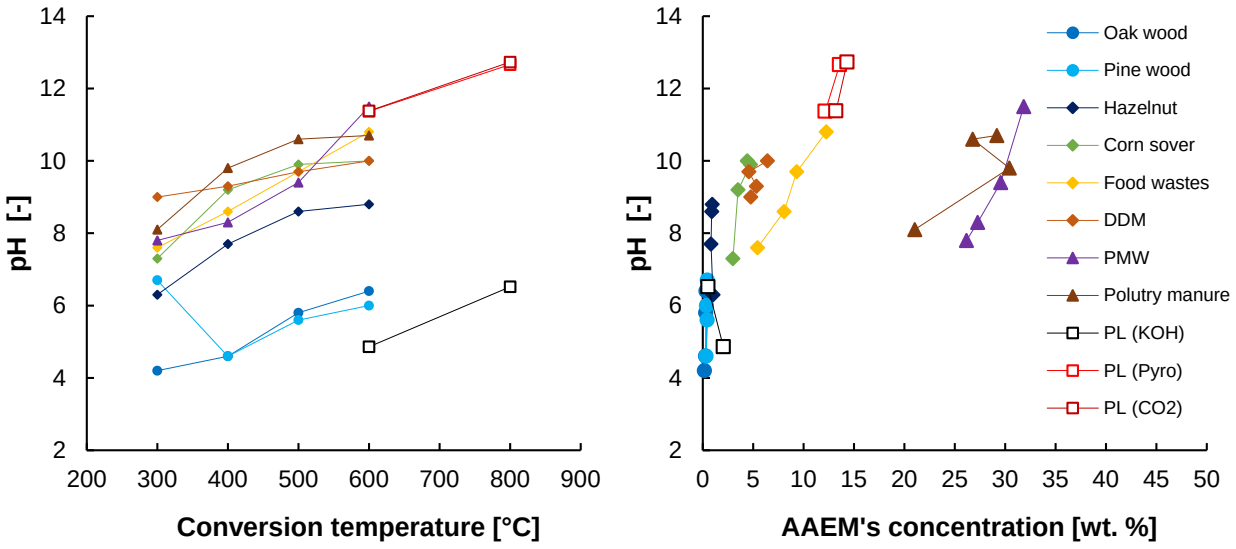

Figure 2. Comparison of influence of conversion temperature (left) and concentration of AAEM's in solids (right) on the pH of its aqueous dispersion (markers: not-filled - this study, filled – DDM – digested diary manure, PMW – paper mill waste) (Enders et al., 2012).

3.2.Structural properties

Activation treatments applied to the WTPL led to significant differences in the results of the specific surface area (SSA) of obtained ACs. As presented in Table 3, the chemical activation with KOH, for both temperatures, caused the development of the largest SSA among all samples. The difference is the most significant for the mesoporous SSA, which at 600 °C is around 19 times higher and at 800 °C around 100 times higher for chemical activation than for the other activation

methods. An interesting behaviour of the samples was observed for the microporous SSA. After activation with KOH, its microporous SSA increased with temperature, but for thermal and physical activation, microporous SSA decreased. It is presumed that the removal of the ash in chemical activation is the major driver of this difference. The WTPL's ash is rich in potassium, calcium and sulphur. According to literature sources, ashes with a high concentration of mentioned elements show a low softening/melting temperature. The thermal processing at temperatures close to the ash softening temperature can lead to a coalescence of the ash with the carbonaceous structure (Mlonka-Mędrala et al., 2020; Niu et al., 2019). For ACs with high ash content (thermal and physical activation), it is suspected that the development of the porous carbon structure of these samples was hindered, mostly by filling/covering the pores, especially at a higher temperature (Kleinhans et al., 2018). The difference in the SSA between thermally and physically activated samples, becomes more significant with an increase in activation temperature, especially for the microporous SSA. It leads to the assumption that the severity of the applied activation conditions was not sufficient since the temperature 600 °C is significantly lower than 710 °C (Kwon et al., 2013; Kwon et al., 2015). On the other hand, at 800 °C the difference is distinguishably higher, which is in a good accordance with the study of Wan et al. (Wan et al., 2019). According to the study of Wan at al. (Wan et al., 2019) the CO_2 can influence on the micropores by two different ways. The CO_2 gasifies the structure of the biomass, which results of formation of the new micropores. In addition, the CO_2 has the ability to crack the volatile compounds and prevents from their deposition on the already formed carbonaceous surface which can cause clogging the entrances to the micropores.

Table 3. Specific surface area of ACs.

Sample	SSA [m^2/g]	
	Micro (< 2 nm)	Meso (2 -50 nm)

KOH-600	991.4	191.0
CO2-600	308.6	10.1
Pyro-600	246.4	7.5
KOH-800	1126.7	1129.5
CO2-800	175.9	15.0
Pyro-800	74.7	10.7

Visible differences between samples investigated in this study can be observed by the SEM images in Figure 3. As it is shown in Figure 3A and Figure 3B the WTPL presents a non-porous structure, in which different structural components can be distinguished, like lignocellulosic biomass (oblong particles), leftovers from protein digestion (spherical particles) and mineral matter (randomly shaped mass). The difference between WTPL activated with KOH at 600 and 800 °C is not strongly visible. Nevertheless, Figure 3C and Figure 3D in comparison to figures of other activation methods indicate a completely different structural morphology. The sharp edges and extensive pores, which are visible for KOH activation, are neither visible for physical nor thermal activation, whose structures have soft edges and no specific porous structure. As it was expected, the initially distinguishable constituent materials in WTPL (Figure 3B) are hard to be noticed for the physical and thermal activation at 800 °C (Figure 3F and Figure 3H). Taking into account that, for low ash containing material, the microporous surface area increased with temperature, it can be suspected that in high ash samples, the mineral material through its softening/melting spills on the structure and tightly plasters part of the surface, filling or covering the entrance to pores.

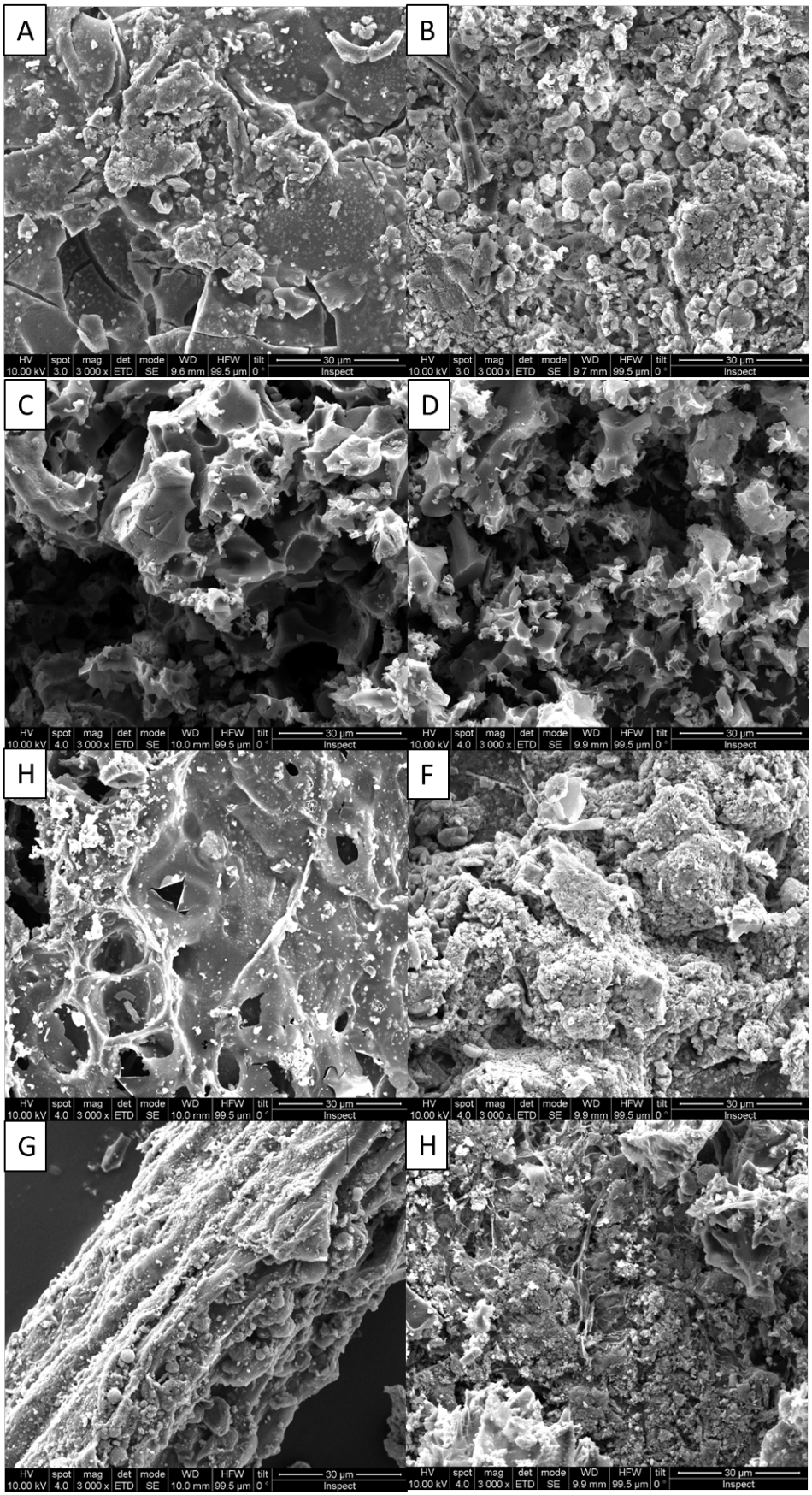
A
B
C
D
H
F
G
H
HV spot mag det mode WD HFW tilt
10.00 kV 3.0 3 000 x ETD SE 9.6 mm 99.5 µm 0 °
30 µm
Inspect
HV spot mag det mode WD HFW tilt
10.00 kV 3.0 3 000 x ETD SE 9.7 mm 99.5 µm 0 °
30 µm
Inspect
HV spot mag det mode WD HFW tilt
10.00 kV 4.0 3 000 x ETD SE 10.0 mm 99.5 µm 0 °
30 µm
Inspect
HV spot mag det mode WD HFW tilt
10.00 kV 4.0 3 000 x ETD SE 9.9 mm 99.5 µm 0 °
30 µm
Inspect
HV spot mag det mode WD HFW tilt
10.00 kV 4.0 3 000 x ETD SE 10.0 mm 99.5 µm 0 °
30 µm
Inspect
HV spot mag det mode WD HFW tilt
10.00 kV 4.0 3 000 x ETD SE 9.9 mm 99.5 µm 0 °
30 µm
Inspect

Figure 3. SEM images, reported at 10.00 kV, a magnification of 3,000x, of produced ACs of raw material (A, B) and activated WTPL chemically: 600 °C (C), 800 °C (D), physically: 600 °C (E), 800 °C (F) and thermally: 600 °C (G), 800 °C (H)

3.3. Adsorption capacity and porous structure

The results of the methylene blue adsorption capacity for all activated materials are shown in Table 4. Along with the processing temperature, the adsorption capacity increases for all types of activation. Similarly to the results of SSA, the WTPL activated with KOH shows much higher adsorption capacity than physically or thermally treated AC. Comparable SSAs for specific temperatures were obtained for physically and thermally activated carbons at both activation temperatures.

Table 4. Adsorption capacity of ACs. Values are expressed as mean (n = 3), standard deviation in brackets.

Activation	T [°C]	q_e [mg/g]
KOH-600	600	675.8 (61.5)
KOH-800	800	872.8 (16.0)
CO2-600	600	135.1 (67.3)
CO2-800	800	236.7 (48.0)
Pyro-600	600	128.6 (38.9)
Pyro-800	800	280.9 (75.3)

The correlation between SSA and absorption capacity presented in Figures 4 and 5 show insight into the relevance of each type of specific surface area. As can be noticed in Figure 4, the relation between micro-SSA and adsorption capacity shows inconsistency. For samples other than chemically activated, the trend shows a decrease in adsorption capacity with an increase of the micro-SSA. Results shown in Figure 5 indicate a correlation between meso-SSA and methylene

blue adsorption capacity. The initial and very steep increase in the absorbed quantity flattens at higher values of mesoporous specific surface area. The logarithmic correlation describes the data in Figure 5 with high accuracy ($R^2 = 0.974$).

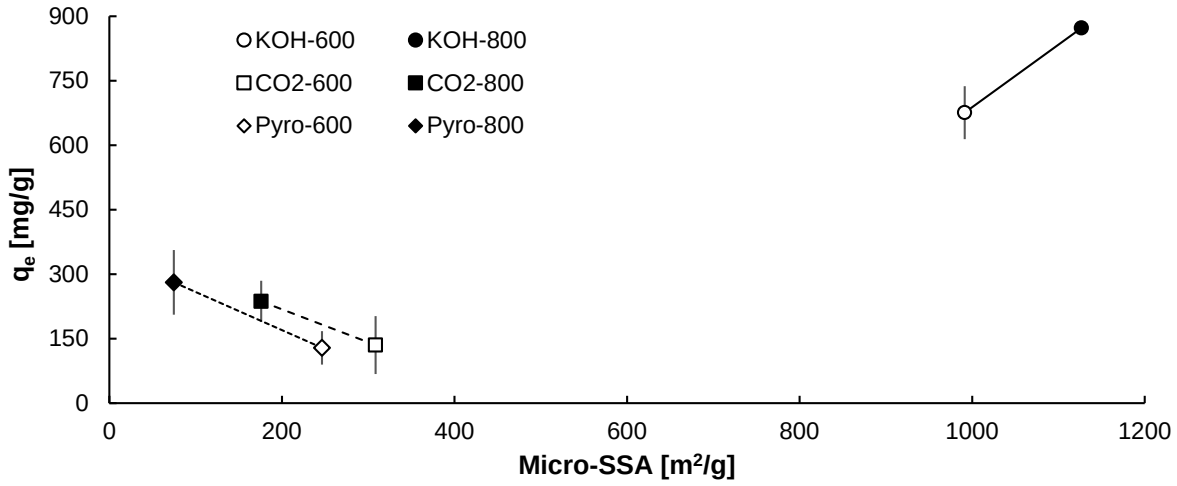

Figure 4. Correlation between adsorption of MB and microporous specific surface area.

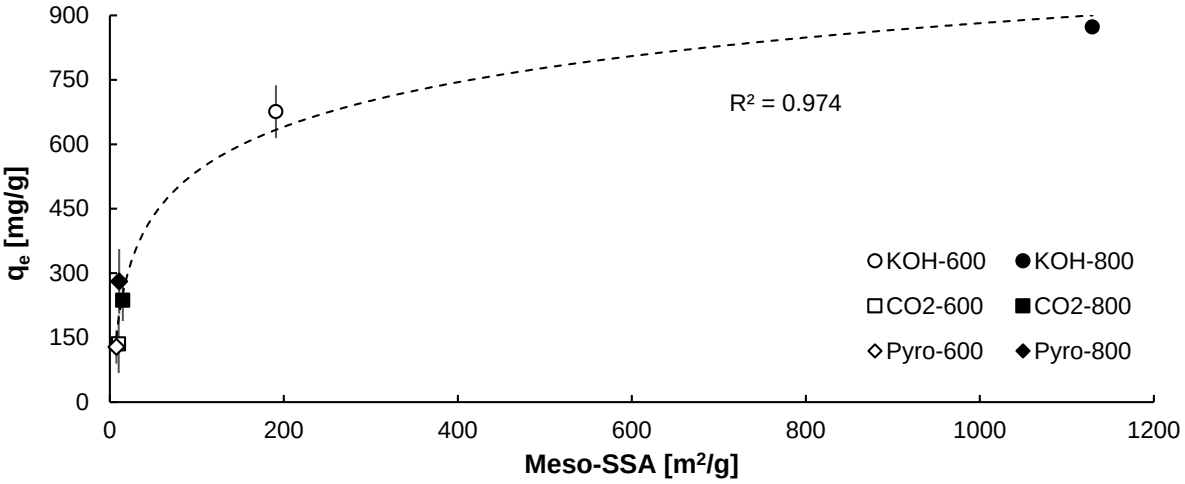

Figure 5. Correlation between adsorption of MB and mesoporous specific surface area.

Resulting correlations between micro and meso SSA and absorbed quantity of MB raise the question of the relevance of micropores in the adsorption of methylene blue. Width, depth, and thickness of a MB molecule are equal to 1.43 nm, 0.61 nm, and 0.40 nm, respectively (Grattan-

Bellew, 2001; Pelekani and Snoeyink, 2000), so its penetration into pores smaller than 2 nm is physically very difficult, if not impossible. Therefore, the correlation of the adsorption of methylene blue with microporous SSA seems to lack a fundamental basis. Figure 5 indicates that pores with sizes between 2 and 50 nm are related to the absorption of the MB, which agrees with other literature sources (Aguiar et al., 2016; Benadjemia et al., 2011; Lladó et al., 2015; Pelekani and Snoeyink, 2000; Reffas et al., 2010). Previous studies also highlight, that in terms of assessment of absorption of anionic and cationic dyes, as well as pharmaceuticals, parameters like pore size distribution, surface functionality, and the pH of the material's water suspension have a significant impact. The study conducted by Aguiar et al. (Aguiar et al., 2016) indicates that the MB's absorption is driven to a great extent by the pore size distribution (PSD) of the material due to the relatively small size of the compound. Vargas et al. (Vargas et al., 2011) state that the strength of the interaction between MB and structural properties of material, on which absorption takes place, can present as the following sequence: π–π dispersion interaction between the aromatic ring of MB and the aromatic structure of the absorptive material > electrostatic interaction between the negatively charged carboxylate anion and the positive charged nitrogen present in MB > proton donor-acceptor interaction between the carbonyl oxygen of pyrones on AC surface and aromatic ring of MB > hydrogen bonds (non-electrostatic interaction). Considering the versatility of the absorption mechanisms, both ACs from activation with KOH can be treated as useful absorbents of compounds, which in their structure have at least one aromatic ring. The WTPL chemically activated at 800 °C shows to be the best suited for water treatment purposes due to its high meso-SSA, high aromatisation level as well as the low ash content and low concentration in heavy metals.

4. Conclusions

The WTPL after activation proved to have potential to be used as the fertilizer or pollutant adsorbent. Depend on the activation method, the inorganic content (nitrogen, potassium, phosphorus) used as the basis of the fertilizers is modified. WTPL activated physically or thermally had satisfactory yields and it consisted higher, nutrient-rich ash content than the initial feedstock. However, the adsorption capacity of both mentioned ACs was relatively low, hindering their possible application in wastewater treatment. In terms of the application as the pollutant adsorbent, the most promising result was obtained for the WTPL activated with KOH. Although, the material produced at 800 °C presented much higher meso-SSA than the one produced at 600 °C, their adsorption capacity of methylene blue was comparable (675.8 mg/g for 600 °C and 872.8 mg/g for 800 °C). Taking also the yields into account, it can be concluded that WTPL activated with KOH in the 600 °C can be indicated as the most technically efficient and economically feasible material for wastewater pollutant adsorption processes. This study shows the possibility of WTPL as useful and valuable feedstock material for valorization into activated carbons. Nevertheless, additional studies on the performance of activated carbons in specific applications would be beneficial for the final evaluation of their suitability.

Acknowledgements

This research was funded by the European Union's Horizon 2020 research and innovation program under the Marie Skłodowska-Curie Grant Agreement No. 721991. We gratefully acknowledge the work of doctoral candidate Ekaterina Ovsyannikova (ICP-OES measurements) and bachelor student Marcel Horn (experimental work assistance).

5. References

Aguiar JE, Oliveira JCA de, Silvino PFG, Neto JA, Silva IJ, Lucena SMP. Correlation between PSD and adsorption of anionic dyes with different molecular weigths on activated carbon. Colloids and Surfaces A: Physicochemical and Engineering Aspects 2016;496:125–31.

Ahmad M, Lee SS, Dou X, Mohan D, Sung J-K, Yang JE et al. Effects of pyrolysis temperature on soybean stover- and peanut shell-derived biochar properties and TCE adsorption in water. Bioresource technology 2012;118:536–44.

Asadullah M, Jahan I, Ahmed MB, Adawiyah P, Malek NH, Rahman MS. Preparation of microporous activated carbon and its modification for arsenic removal from water. Journal of Industrial and Engineering Chemistry 2014;20(3):887–96.

Atimtay A, Yurdakul S. Combustion and Co-Combustion characteristics of torrefied poultry litter with lignite. Renewable Energy 2020;148:1292–301.

Benadjemia M, Millière L, Reinert L, Benderdouche N, Duclaux L. Preparation, characterization and Methylene Blue adsorption of phosphoric acid activated carbons from globe artichoke leaves. Fuel Processing Technology 2011;92(6):1203–12.

Benstoem F, Becker G, Firk J, Kaless M, Wuest D, Pinnekamp J et al. Elimination of micropollutants by activated carbon produced from fibers taken from wastewater screenings using hydrothermal carbonization. Journal of environmental management 2018;211:278–86.

Bourke J, Manley-Harris M, Fushimi C, Dowaki K, Nunoura T, Antal MJ. Do All Carbonized Charcoals Have the Same Chemical Structure?: 2. A Model of the Chemical Structure of Carbonized Charcoal †. Ind. Eng. Chem. Res. 2007;46(18):5954–67.

Cantrell KB, Hunt PG, Uchimiya M, Novak JM, Ro KS. Impact of pyrolysis temperature and manure source on physicochemical characteristics of biochar. Bioresource technology 2012;107:419–28.

Cao X, Harris W. Properties of dairy-manure-derived biochar pertinent to its potential use in remediation. Bioresource technology 2010;101(14):5222–8.

Chan KY, Dorahy CG, Tyler S, Wells AT, Milham PP, Barchia I. Phosphorus accumulation and other changes in soil properties as a consequence of vegetable production, Sydney region, Australia. Australian Journal of Soil Research 2007;45(2):139.

Chan KY, van Zwieten L, Meszaros I, Downie A, Joseph S. Using poultry litter biochars as soil amendments. Soil Res. 2008;46(5):437.

Cimò G, Kucerik J, Berns AE, Schaumann GE, Alonzo G, Conte P. Effect of heating time and temperature on the chemical characteristics of biochar from poultry manure. Journal of agricultural and food chemistry 2014;62(8):1912.

Dissanayake PD, Choi SW, Igalavithana AD, Yang X, Tsang DCW, Wang C-H et al. Sustainable gasification biochar as a high efficiency adsorbent for CO2 capture: A facile method to designer biochar fabrication. Renewable and Sustainable Energy Reviews 2020;124:109785.

Dwivedi P, Gaur V, Sharma A, Verma N. Comparative study of removal of volatile organic compounds by cryogenic condensation and adsorption by activated carbon fiber. Separation and Purification Technology 2004;39(1):23–37.

E. D. Vories, T. A. Costello, R. E. Glover. Runoff from cotton fields fertilized with poultry litter. Transactions of the ASAE 2001;44(6).

Enders A, Hanley K, Whitman T, Joseph S, Lehmann J. Characterization of biochars to evaluate recalcitrance and agronomic performance. Bioresource technology 2012;114:644–53.
Font-Palma C. Characterisation, kinetics and modelling of gasification of poultry manure and litter: An overview. Energy Conversion and Management 2012;53(1):92–8.
Freihardt J, Jekel M, Ruhl AS. Comparing test methods for granular activated carbon for organic micropollutant elimination. Journal of Environmental Chemical Engineering 2017;5(3):2542–51.
Giudicianni P, Cardone G, Ragucci R. Cellulose, hemicellulose and lignin slow steam pyrolysis: Thermal decomposition of biomass components mixtures. Journal of Analytical and Applied Pyrolysis 2013;100:213–22.
Grattan-Bellew PE. Petrographic and Technological Methods for Evaluation of Concrete Aggregates-2; 2001.
Hossain MK, Strezov V, Chan KY, Ziolkowski A, Nelson PF. Influence of pyrolysis temperature on production and nutrient properties of wastewater sludge biochar. Journal of environmental management 2011;92(1):223–8.
Ippolito JA, Spokas KA, Novak JM, Lentz RD, Cantrell KB. Biochar elemental composition and factors influencing nutrient retention: Routledge, 2015. Biochar for environmental management: Science, technology and implementation.
Isemin RL, Mikhalev AV, Muratova NS, Kogh-Tatarenko VS, Teplitskii YS, Buchilko EK et al. Improving the Efficiency of Biowaste Torrefaction. Therm. Eng. 2019;66(7):521–6.
J. W. Gaskin, C. Steiner, K. Harris, K. C. Das, B. Bibens. Effect of Low-Temperature Pyrolysis Conditions on Biochar for Agricultural Use. Transactions of the ASABE 2008;51(6):2061–9.
Jeffrey M. Novak, Isabel Lima, Baoshan Xing, Julia W. Gaskin, Christoph Steiner, K. C. Das et al. Characterization of Designer Biochar Produced at Different Temperatures and Their Effects on a Loamy Sand.
Katsaros G, Pandey DS, Horvat A, Aranda Almansa G, Fryda LE, Leahy JJ et al. Experimental investigation of poultry litter gasification and co-gasification with beech wood in a bubbling fluidised bed reactor – Effect of equivalence ratio on process performance and tar evolution. Fuel 2020;262:116660.
Keiluweit M, Nico PS, Johnson MG, Kleber M. Dynamic molecular structure of plant biomass-derived black carbon (biochar). Environmental science & technology 2010;44(4):1247–53.
Kleinhans U, Wieland C, Frandsen FJ, Spliethoff H. Ash formation and deposition in coal and biomass fired combustion systems: Progress and challenges in the field of ash particle sticking and rebound behavior. Progress in Energy and Combustion Science 2018;68(C):65–168.
Kwon EE, Cho S-H, Kim S. Synergetic sustainability enhancement via utilization of carbon dioxide as carbon neutral chemical feedstock in the thermo-chemical processing of biomass. Environmental science & technology 2015;49(8):5028–34.
Kwon EE, Jeon E-C, Castaldi MJ, Jeon YJ. Effect of carbon dioxide on the thermal degradation of lignocellulosic biomass. Environmental science & technology 2013;47(18):10541–7.
Landers J, Gor GY, Neimark AV. Density functional theory methods for characterization of porous materials. Colloids and Surfaces A: Physicochemical and Engineering Aspects 2013;437(C):3–32.

Li H, Li Y, Xu Y, Lu X. Biochar phosphorus fertilizer effects on soil phosphorus availability. Chemosphere 2020;244:125471.
Lladó J, Lao-Luque C, Ruiz B, Fuente E, Solé-Sardans M, Dorado AD. Role of activated carbon properties in atrazine and paracetamol adsorption equilibrium and kinetics. Process Safety and Environmental Protection 2015;95(C):51–9.
Lowell S. Characterization of porous solids and powders: Surface area, pore size, and density. Dordrecht, Boston: Dordrecht; Boston Kluwer Academic Publishers, 2004.
Mau V, Arye G, Gross A. Wetting properties of poultry litter and derived hydrochar. PloS one 2018;13(10):e0206299.
McBeath AV, Smernik RJ, Krull ES, Lehmann J. The influence of feedstock and production temperature on biochar carbon chemistry: A solid-state 13C NMR study. Biomass and Bioenergy 2014;60:121–9.
Mlonka-Mędrala A, Magdziarz A, Gajek M, Nowińska K, Nowak W. Alkali metals association in biomass and their impact on ash melting behaviour. Fuel 2020;261.
Mukome FND, Zhang X, Silva LCR, Six J, Parikh SJ. Use of chemical and physical characteristics to investigate trends in biochar feedstocks. Journal of agricultural and food chemistry 2013;61(9):2196.
Nazem MA, Zare MH, Shirazian S. Preparation and optimization of activated nano-carbon production using physical activation by water steam from agricultural wastes. RSC Adv. 2020;10(3):1463–75.
Nishimiya K, Hata T, Imamura Y, Ishihara S. Analysis of chemical structure of wood charcoal by X-ray photoelectron spectroscopy. Journal of Wood Science 1998(1):56–61.
Niu Y, Lv Y, Lei Y, Liu S, Liang Y, Wang D et al. Biomass torrefaction: Properties, applications, challenges, and economy. Renewable and Sustainable Energy Reviews 2019;115.
Oginni O, Singh K, Oporto G, Dawson-Andoh B, McDonald L, Sabolsky E. Effect of one-step and two-step H3PO4 activation on activated carbon characteristics. Bioresource Technology Reports 2019;8:100307.
Osman AI, Blewitt J, Abu-Dahrieh JK, Farrell C, Al-Muhtaseb A'aH, Harrison J et al. Production and characterisation of activated carbon and carbon nanotubes from potato peel waste and their application in heavy metal removal. Environmental science and pollution research international 2019;26(36):37228–41.
Otowa T, Nojima Y, Miyazaki T. Development of KOH activated high surface area carbon and its application to drinking water purification. Carbon 1997;35(9):1315–9.
Ovsyannikova E, Arauzo PJ, Becker GC, Kruse A. Experimental and thermodynamic studies of phosphate behavior during the hydrothermal carbonization of sewage sludge. Science of the Total Environment 2019;692:147–56.
Pelekani C, Snoeyink VL. Competitive adsorption between atrazine and methylene blue on activated carbon: The importance of pore size distribution. Carbon 2000;38(10):1423–36.
Pituello C, Francioso O, Simonetti G, Pisi A, Torreggiani A, Berti A et al. Characterization of chemical–physical, structural and morphological properties of biochars from biowastes produced at different temperatures. J Soils Sediments 2015;15(4):792–804.
Pizarro MD, Céccoli G, Muñoz FF, Frizzo LS, Daurelio LD, Bouzo CA. Use of raw and composted poultry litter in lettuce produced under field conditions: Microbiological quality and safety assessment. Poultry Science 2019;98(6):2608–14.

Plaza MG, González AS, Pevida C, Pis JJ, Rubiera F. Valorisation of spent coffee grounds as CO2 adsorbents for postcombustion capture applications. Applied Energy 2012;99:272–9.
Powell S, Johnston S, Gaston L, Southern LL. The Effect of Dietary Phosphorus Level and Phytase Supplementation on Growth Performance, Bone-Breaking Strength, and Litter Phosphorus Concentration in Broilers 1. Poultry Science 2008;87(5):949–57.
Prahas D, Kartika Y, Indraswati N, Ismadji S. Activated carbon from jackfruit peel waste by H3PO4 chemical activation: Pore structure and surface chemistry characterization. Chemical Engineering Journal 2008;140(1-3):32–42.
Rashidi NA, Yusup S. Potential of palm kernel shell as activated carbon precursors through single stage activation technique for carbon dioxide adsorption. Journal of Cleaner Production 2017;168:474–86.
Ravikovitch PI, Vishnyakov A, Russo R, Neimark AV, Tri/Princeton N. Unified approach to pore size characterization of microporous carbonaceous materials from N{sub 2}, Ar, and CO{sub 2} adsorption isotherms. Langmuir 2000;16(5).
Reffas A, Bernardet V, David B, Reinert L, Lehocine MB, Dubois M et al. Carbons prepared from coffee grounds by H 3PO 4 activation: Characterization and adsorption of methylene blue and Nylosan Red N-2RBL. Journal of hazardous materials 2010;175(1-3):779–88.
Rodriguez Correa C, Hehr T, Voglhuber-Slavinsky A, Rauscher Y, Kruse A. Pyrolysis vs. hydrothermal carbonization: Understanding the effect of biomass structural components and inorganic compounds on the char properties. Journal of Analytical and Applied Pyrolysis 2019;140:137–47.
Rodriguez Correa C, Otto T, Kruse A. Influence of the biomass components on the pore formation of activated carbon. Biomass and Bioenergy 2017;97:53–64.
Rodríguez Correa C, Ngamying C, Klank D, Kruse A. Investigation of the textural and adsorption properties of activated carbon from HTC and pyrolysis carbonizates. Biomass Conv. Bioref. 2018;8(2):317–28.
Ronsse F, Nachenius RW, Prins W. Carbonization of Biomass, Recent Advances in Thermo-Chemical Conversion of Biomass 2015.
Saleem J, Shahid UB, Hijab M, Mackey H, McKay G. Production and applications of activated carbons as adsorbents from olive stones. Biomass Conv. Bioref. 2019;9(4):775–802.
Santos Dalólio F, da Silva JN, Carneiro de Oliveira AC, Ferreira Tinôco IdF, Christiam Barbosa R, Resende MdO et al. Poultry litter as biomass energy: A review and future perspectives. Renewable and Sustainable Energy Reviews 2017;76:941–9.
Shankar Pandey D, Kwapinska M, Leahy JJ, Kwapinski W. Fly Ash From Poultry Litter Gasification – Can it be Utilised in Agriculture Systems as a Fertiliser? Energy Procedia 2019;161:38–46.
Silvestre-Albero J, Silvestre-Albero A, Rodríguez-Reinoso F, Thommes M. Physical characterization of activated carbons with narrow microporosity by nitrogen (77.4K), carbon dioxide (273K) and argon (87.3K) adsorption in combination with immersion calorimetry. Carbon 2012;50(9):3128–33.
Suhas, Carrott PJM, Ribeiro Carrott MML. Lignin--from natural adsorbent to activated carbon: A review. Bioresource technology 2007;98(12):2301–12.
Tang Y-H, Liu S-H, Tsang DCW. Microwave-assisted production of CO2-activated biochar from sugarcane bagasse for electrochemical desalination. Journal of hazardous materials 2020;383.

Vargas AMM, Cazetta AL, Kunita MH, Silva TL, Almeida VC. Adsorption of methylene blue on activated carbon produced from flamboyant pods (Delonix regia): Study of adsorption isotherms and kinetic models. Chemical Engineering Journal 2011;168(2):722–30.
Vassilev SV, Baxter D, Andersen LK, Vassileva CG. An overview of the chemical composition of biomass. Fuel 2010;89(5):913–33.
Wan Z, Sun Y, Tsang DCW, Yu IKM, Fan J, Clark JH et al. A sustainable biochar catalyst synergized with copper heteroatoms and CO 2 for singlet oxygenation and electron transfer routes. Green Chemistry 2019;21(17):4800–14.
Wang D, Geng Z, Li B, Zhang C. High performance electrode materials for electric double-layer capacitors based on biomass-derived activated carbons. Electrochimica Acta 2015;173:377–84.
Wang L, Bolan NS, Tsang DCW, Hou D. Green immobilization of toxic metals using alkaline enhanced rice husk biochar: Effects of pyrolysis temperature and KOH concentration. The Science of the total environment 2020;720:137584.
Weber K, Quicker P. Properties of biochar. Fuel 2018;217:240.
Wei X-q, Li Q-h, Li H-c, Li H-j, Chen S-x. The use of ZnCl2 activation to prepare low-cost porous carbons coated on glass fibers using mixtures of Novolac, polyethylene glycol and furfural as carbon precursors. New Carbon Materials 2015;30(6):579–86.
Yang G, Wang Z, Xian Q, Shen F, Sun C, Zhang Y et al. Effects of pyrolysis temperature on the physicochemical properties of biochar derived from vermicompost and its potential use as an environmental amendment. RSC Adv. 2015;5(50):40117–25.
Yang H, Yan R, Chen H, Lee DH, Zheng C. Characteristics of hemicellulose, cellulose and lignin pyrolysis. Fuel 2007;86(12):1781–8.
Yu IKM, Xiong X, Tsang DCW, Wang L, Hunt AJ, Song H et al. Aluminium-biochar composites as sustainable heterogeneous catalysts for glucose isomerisation in a biorefinery. Green Chemistry 2019;21(6):1267–81.
Zhu X-L, Wang P-Y, Peng C, Yang J, Yan X-B. Activated carbon produced from paulownia sawdust for high-performance CO2 sorbents. Chinese Chemical Letters 2014;25(6):929–32.

Supplementary information for

Valorization of the poultry litter through wet torrefaction and different activation treatments

P. J. Arauzo [a]*, P. A. Maziarka [b], M. P. Olszewski[a], R. L. Isemin[c], N. S. Muratova[c], F. Ronsse[b], A. Kruse[a]

Address:

[a]Department of Conversion Technologies of Biobased Resources, Institute of Agricultural Engineering, University of Hohenheim, Garbenstrasse 9, DE-70599 Stuttgart, Germany

[b]Department of Green Chemistry and Technology, Faculty of Bioscience Engineering, Ghent University, Coupure Links 653, 9000 Gent, Belgium

[c]Biocenter, Tambov State Technical University, Ulitsa Leningradskaya, 1, Tambov, 392036, Russia

Figure captions

Fig A1. FT-IR of initial wet torrefied poultry litter.

Fig A2. Scheme of the activated carbon device used during the physical and thermal treatments at the facility at the University of Hohenheim, Stuttgart, Germany.

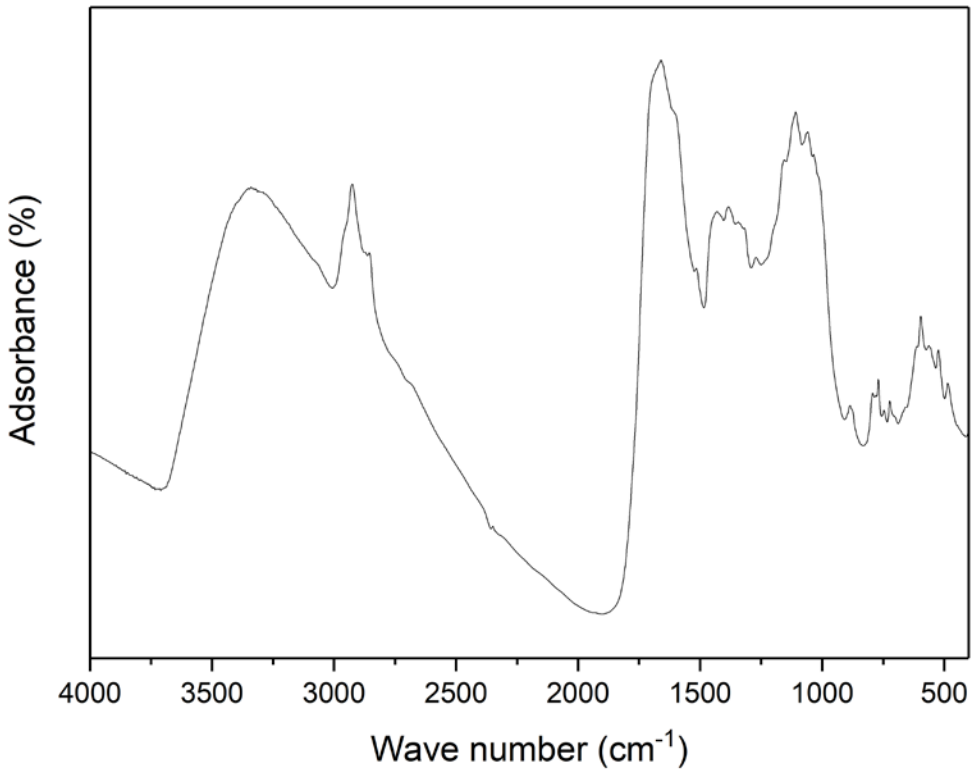

Fig A1. FT-IR of initial wet torrefied poultry litter.

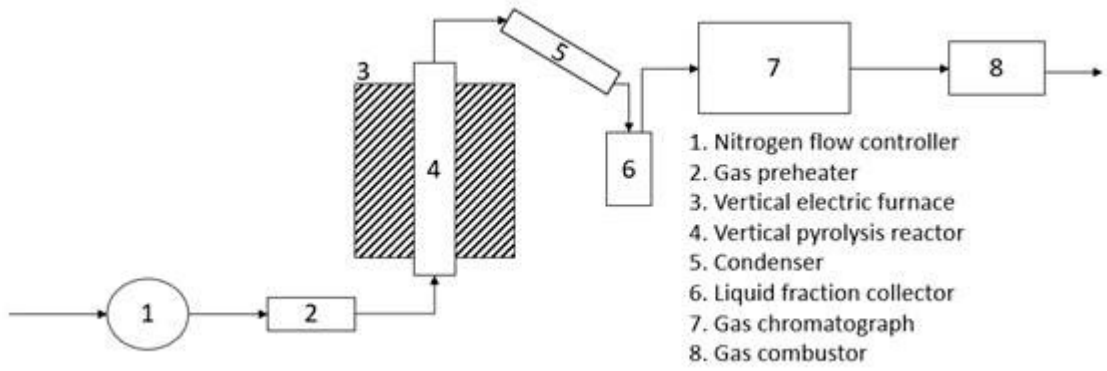

Fig A2. Scheme of the activated carbon device used during the physical and thermal treatments at the facility at the University of Hohenheim, Stuttgart, Germany.